NJC

Accepted Manuscript

ROYAL SOCIETY OF CHEMISTRY

rsc.li/njc

View Article Online
DOI: 10.1039/C6NJ03070J

Journal Name

ARTICLE

White light emission from simple AIE-ESIPT-Excimer tripled single molecular system

Received 00th January 20xx,
Accepted 00th January 20xx

DOI: 10.1039/x0xx00000x

www.rsc.org/

Soham Samanta, Utsab Manna and Gopal Das*

A simple organic molecule (**L_3**) has been systematically designed and developed to generate white light emission from a single component system. It also could tune several emission colors due to its diverse spectral nature with varying water fractions in methanol-water mixture and acetonitrile-water mixture. Essentially introducing aggregation-induced emission (AIE) phenomenon and Excimer formation ability in the molecular system provided the scope for dual emission whereas ESIPT (excited state intramolecular proton transfer) coupled-AIE phenomenon worked as an additional handle to adjust emission wavelength of the corresponding emission peak by varying solvent polarity. Detailed AFM (atomic force microscope), DLS (dynamic light scattering) and X-ray crystallographic studies were carried out to validate the mechanism of white light emission output.

Introduction

In recent time, white-light-emitting organic materials and devices have grabbed the limelight due to their various important lighting applications. To achieve an ideal white-light emission a system requires either simultaneous emission of three primary RGB (red, green and blue) colors or at least two complementary colors having almost similar distribution of emission intensities covering the entire visible wavelength (400 to 700 nm) region.[1] Hence, most of the reported white-light emitters deal with combination of several components having different emission output colors covering the entire visible spectrum.[2-7] However, generating white-light emission from the combination of multiple components is a relatively complicated process with much less stability. Compared to these multicomponent white-light emitters, a single white-light-emitting organic molecule could offer advantages in terms of its improved stability and reproducibility, as well as a simpler fabrication process.[8-11] However, examples of acquiring white-light emission from a single organic molecule are very handful.

Most recently, organic molecules having aggregation induced emission (AIE) or aggregation induced emission enhancement (AIEE)[12-13] and excited state intramolecular proton transfer (ESIPT),[14-15] properties are being extensively used for generating tunable luminescence responses. Fluorescent organic molecules that can display aggregation-induced emission (AIE) properties have come to the limelight as these molecules display weak emission in dilute solutions, which is enhanced dramatically due to aggregation of the fluorophore species in solution or in the solid state. Usually AIE or AIEE is explained by restriction of intramolecular rotation (RIR), intramolecular charge-transfer (ICT), excimer formation, and excited-state proton-transfer (ESPT) processes.[16-18] Although the RIR and ICT processes has already been studied exclusively in explaining the AIE phenomenon, ESPT theory discussed seldom in this regard. Even though a few articles referred to ESIPT theory, they failed to elucidate AIE behavior in the light of excited-state proton-transfer (ESIPT) process in depth by investigating crystal structures. More often, multiple color emission can be achieved from AIE or AIEE responsive single molecules due to different conformation and/or packing modes in the aggregated state, or due to a change in the degree of aggregation which may lead to white light emission.[19-20]

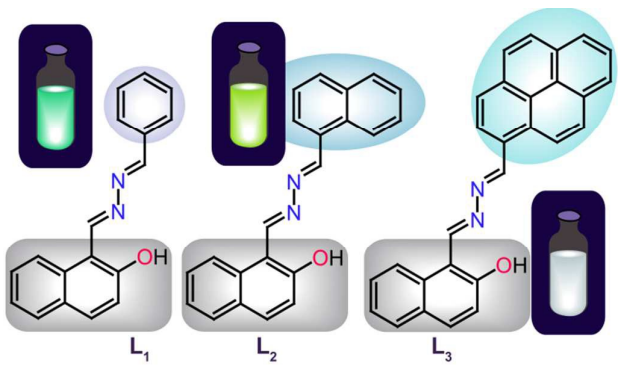

Scheme 1: Designing of L_1, L_2 and L_3

Moreover, as pyrene more often indulges in self-assembly to assimilate excimer emission, introducing pyrene moiety in a

Department of Chemistry, Indian Institute of Technology Guwahati, Assam - 781039, India. Fax: + 91 361 2582349; Tel: +91 3612582313; E-mail: gdas@iitg.ernet.in.

†Electronic Supplementary Information (ESI) available: NMR, HRMS characterization spectra of the synthesized organic molecules, supporting plot and figures, DLS spectra, AFM images. See DOI: 10.1039/x0xx00000x

View Article Online
DOI: 10.1039/C6NJ03070J

AIE-ESIPT coupled system might provide an additional emission peak in aggregated form.[21-22] Hence, designing AIE-ESIPT coupled simple organic molecules with suitable combination of fluorophore could open up the scope for achieving tunable white light emission. However thorough literature study revealed that the possibility of designing simple organic molecule with the abilities of showing AIE, ESIPT and excimer formation together rarely explored till date. Thus, in our continuous pursuit to develop various fluorogenic systems[23-30] with several optical applications in the present manuscript we would like to discuss systematic development of AIE active bis-imine molecules (**L_1**, **L_2** and **L_3**) with interesting ESIPT properties to achieve pure white light emission from single organic molecule system by suitable variation of fluorophoric units (Scheme 1).

Experimental

General Information and Materials

All the materials for synthesis were purchased from commercial suppliers and used without further purification. The absorption spectra were recorded on a Perkin-Elmer Lamda-25 UV–vis spectrophotometer using 10 mm quartz cuvettes. Fluorescence measurements were performed on a Horiba Fluoromax-4 using 10 mm path length cuvettes with a slit width of 3 nm at 298 K. The mass spectra were obtained using Waters Q-ToF Premier mass spectrometer. NMR spectra were recorded on a Bruker Advance 600 MHz instrument. The chemical shifts were recorded in parts per million (ppm) scale. The following abbreviations are used to describe spin multiplicities in ^{1}H NMR spectra: s = singlet; d = doublet; t = triplet; m = multiplet.

Synthesis of L_1

Following reported procedure 1-(hydrazonomethyl)naphthalene-2-ol was synthesized (Step 1, scheme 2).[23] In Step 2, 1.0 mmol of this product was mixed with 1.1 mmol of benzaldehyde and stirred for 12 h to obtain a pale yellow colored solid product. The product was then filtered, washed thoroughly with methanol and eventually dried in a desiccator. Calculated yield: 86%. ^{1}H NMR [600 MHz, $CDCl_3$, TMS, *J* (Hz), δ (ppm)]: 13.37 (1H, s), 9.73 (1H, s), 8.69 (1H, s), 8.19 (1H, d, *J*=8.4), 7.86-7.90 (3H, m), 7.81 (1H, d, *J*=8.4), 7.58 (1H, t, *J*=7.2), 7.51-7.49 (3H, m), 7.41 (1H, t, *J*=7.2), 7.27 (1H, d, *J*=15.0). ^{13}C NMR [150 MHz, $CDCl_3$, TMS, δ (ppm)]: 161.69, 161.59, 161.27, 134.65, 133.80, 132.87, 131.58, 129.22, 128.98, 128.72, 128.22, 127.94, 123.74, 120.15, 120.23, 119.28, 108.32. ESI-MS (positive mode, m/z) Calculated for $C_{18}H_{14}N_2O$: 275.1184. Found: 275.1154 [$(M+H^+)$].

Synthesis of L_2

L_2 was synthesized using a similar procedure like **L_1**, wherein only 1-naphthaldehyde was used in place of benzaldehyde (Scheme 2). Calculated yield: 83%. ^{1}H NMR [600 MHz, $CDCl_3$, TMS, *J* (Hz), δ (ppm)]: 13.45 (1H, s), 9.83 (1H, s), 9.32 (1H, s), 8.96 (1H, d, *J*=8.4), 8.22 (1H, d, *J*=8.4), 8.10 (1H, d, *J*=6.6), 8.00 (1H, d, *J*=7.8), 7.94 (1H, d, *J*=7.8), 7.88 (1H, d, *J*=9.0), 7.81 (1H, d, *J*=8.4), 7.69 (1H, t, *J*=7.8), 7.60-7.58 (3H, m), 7.41 (1H, t, *J*=7.2), 7.27 (1H, d, *J*=10.2). ^{13}C NMR [150 MHz, $CDCl_3$, TMS, δ (ppm)]: 161.86, 161.59, 161.46, 134.81, 134.15, 133.03, 132.43, 131.54, 129.91, 129.49, 129.38, 129.11, 128.39, 128.10, 127.80, 126.61, 125.57, 124.79, 123.90, 120.36, 119.46, 108.54. ESI-MS (positive mode, m/z) Calculated for $C_{22}H_{16}N_2O$: 325.1340. Found: 325.1300 [$(M+H^+)$].

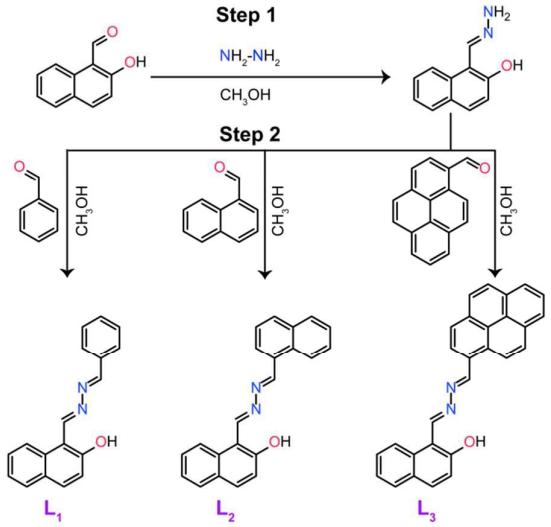

Scheme 2: Synthesis of **L_1**, **L_2** and **L_3**

Synthesis of L_3

L_3 was synthesized using a similar procedure like **L_1**, wherein only 1-Pyrenecarboxaldehyde was used in place of benzaldehyde (Scheme 2). Needle shaped orange crystal was obtained from DCM at room temperature.
Calculated yield: 76%. ^{1}H NMR [600 MHz, $CDCl_3$, TMS, *J* (Hz), δ (ppm)]: 13.531 (1H, s) or 13.00 (1H*, s), 9.86 (1H, s) or 9.63 (1H*, s), 9.67 (1H, s), 8.91 (1H, d, *J*=9.0), 8.72 (1H, d, *J*=7.8), 8.26-8.23 (5H, m), 8.17 (1H, d, *J*=9.6), 8.10 (1H, d, *J*=7.8), 8.06 (1H, t, *J*=7.2), 7.88 (1H, d, *J*=8.4), 7.81 (1H, d, *J*=7.8), 7.60 (1H, t, *J*=7.2), 7.42 (1H, t, *J*=7.2), 7.29 (1H, d, *J*=9.0). ^{13}C NMR [150 MHz, $CDCl_3$, TMS, δ (ppm)]: 161.63, 161.51, 161.40, 135.15, 134.78, 133.84, 133.05, 131.46, 130.81, 130.77, 129.39, 128.41, 128.10, 127.64, 126.59, 126.52, 126.33, 125.29, 125.19, 124.76, 123.90, 122.85, 120.39, 119.47, 119.35. ESI-MS (positive mode, m/z) Calculated for $C_{28}H_{18}N_2O$: 399.1497. Found: 399.1528 [$(M+H^+)$].

Crystallographic Refinement Details

Intensity data for the all crystals were collected Mo-Kα radiation (λ = 0.71073Å) at 298(2) K, with increasing ω (width of 0.3° per frame) at a scan speed of 6 s/ frame on a Bruker SMART APEX diffractometer equipped with CCD area detector. The data integration and reduction were processed with SAINT[31] software. An empirical absorption correction was

View Article Online
DOI: 10.1039/C6NJ03070J

applied to the collected reflections with SADABS.[32] The structures were solved by direct methods using SHELXTL[33] and were refined on F^2 by the full-matrix least-squares technique using the SHELXL-97 program package.[34] Graphics are generated using MERCURY 3.0.[35] Non-hydrogen atoms are treated anisotropically. The hydrogen atoms are geometrically fixed.

CCDC No. 1434540, Formula - $C_{28}H_{18}N_2O$, Fw - 398.44, Crystal system – monoclinic, Space group *P* 21, a = 9.6949(8) Å, b = 16.3365(19) Å, c = 12.5230(1) Å, α = 90°, β = 96.097°(8), γ = 90°, V = 2056 Å^3, Z = 4, D_c = 1.342 g cm^{-3}, μ (MoKα) = 10.082 mm^{-1}, F(000) = 832.0, T = 298(2) K, $\theta_{max.}$ = 26.99, Total no. of reflections = 8784, Independent reflections = 7079, Observed reflections = 3947, Parameters refined = 561, Flack parameters = -3.9(10), R_1, I > 2σ(I) = 0.1277, wR_2, I > 2σ(I) = 0.3054, GOF (F^2) = 1.189.

UV–Vis and fluorescence spectroscopic studies

Stock solutions of **L_1** and **L_2** (5×10^{-3} mol. L^{-1}) were prepared in DMSO. The solution of **L_1** or **L_2** was then diluted to 10×10^{-6} mol. L^{-1} for fluorescence spectral studies with CH_3OH/aqueous mixed solvents having different water fractions (varied from 0-100%). However, for UV-Visible experiments the final concentration of the experimental solutions of **L_1** or **L_2** were adjusted at 25 μM by diluting the respective stock solutions. On the other hand, a stock solution of **L_3** was also prepared in DMSO having concentration 1.25×10^{-3} mol. L^{-1}. The solution of **L_3** was then diluted to 10×10^{-6} mol. L^{-1} for spectral studies (both UV-Visible and fluorescence) by taking only 16 μL stock solution of the molecule and making the final volume 2 mL adding CH_3OH/aqueous or THF/aqueous or CH_3CN/aqueous mixed solvents with different water fractions (varied from 0-100%). Fluorescence and UV-visible experiments were carried out in quartz optical cells of 1 cm path length.

Dynamic light scattering studies

Dynamic light scattering (DLS) experiments were performed on a Malvern Zetasizer Nano ZS instrument equipped with a 4.0 mW He–Ne laser operating at a wavelength of 633 nm at room temperature. It was carried out with optically clear solutions of **L_1**, **L_2** and **L_3** (10 μM) in 5:5 MeOH-H_2O and 1:9 MeOH-H_2O mixed solvents to observe the change in particle size upon increasing water fraction. The solutions were equilibrated for 30 minutes before taking the measurements.

Atomic Force Microscope (AFM) Studies

The morphology of the aggregates were investigated from NT-MDT micro-40 AFM instrument using a semi-contact mode at a scan rate of 1 Hz. Solutions of **L_1**, **L_2** and **L_3** (10 μM) in 1:9 MeOH-H_2O mixed solvent were respectively drop-casted on three different cover slips and left open to atmosphere for 12 h, followed by desiccation prior to acquiring AFM images. For **L_3** (10 μM) another AFM image was taken wherein a solution of **L_3** (10 μM) in 1:9 THF-H_2O mixed solvent was drop-casted on a cover slip.

Results and discussion

Rationale behind the design of L_1, L_2 and L_3:

Schiff base compounds **L_1**, **L_2** and **L_3** were rationally designed and synthesized in order to achieve tunable white light emission (Scheme 1&2). Essentially the idea to keep bis-imine core intact along with naphthol moiety in all **L_1**, **L_2** and **L_3** was fundamentally based on the theory that it would inherently introduce AIE behavior in these types of compounds likewise our previously reported AIE active systems.[23, 25] Eventually this AIE active behavior would allow the system to show high fluorescence. However, it was necessary to link AIE phenomenon with dual emission behavior (comprised of complementary emission colors) to achieve white light. Hence we systematically introduced the additional phenyl (in **L_1**) or naphthyl (**L_2**) or pyrene (in **L_3**) moiety to acquire extra emission peak. These variation of the phenyl (in **L_1**) or naphthyl (**L_2**) or pyrene (in **L_3**) moiety was based on the fundamental notion that unlike the phenyl (in **L_1**) or naphthyl (**L_2**) moiety introducing pyrene (in **L_3**) moiety would generate a distinct extra emission peak due to its tendency to form excimer. Moreover, we also envisaged that imine-naphthol excited state intramolecular proton transfer could be instrumental in acquiring solvent polarity dependent emission maxima (generated due to AIE) shift.

UV-Visible spectroscopic study of L_1, L_2 and L_3:

The UV-Vis spectra of **L_1**, **L_2** and **L_3** (25 μM, 25 μM and 10 μM respectively) in pure methanol revealed sharp absorbance maxima at 379, 387 and 416 nm respectively which may be attributed to the π-π* charge transfer transitions of the concerned molecules (Figure S11, ESI). It was interesting to note that gradual addition of water into its methanol solution led to regular decrease of the absorption bands for **L_1**, **L_2** and **L_3** likely due to the formation of molecular aggregates (Figure S11, ESI). Absorption spectra taken with varying water fraction in a methanol-water mixture too revealed that gradual increase in the water fraction could result in the systematic reduction of the absorbance peak accompanied by ~10-12 nm red shifts for every molecular system (**L_1**, **L_2** and **L_3**). Eventually UV-Vis spectra of **L_1**, **L_2** and **L_3** in the methanol-water mixed solvents with higher water fractions (>60%) also witnessed increase in the base lines which also reiterated the formation of aggregates (Figure S11, ESI). Hence initially it was anticipated that each of the designed molecules **L_1**, **L_2** and **L_3** might exhibit aggregation induced emission property.[36]

Studies of AIE (aggregation-induced emission) properties of L_1& L_2:

All the three designed organic molecules (**L_1**, **L_2** and **L_3**) were found to be very weakly emissive in pure methanol. However, it was interesting to note that these weakly emissive **L_1**, **L_2** and **L_3** in methanol became highly emissive in a methanol–water mixture with higher water contents (Figure 1 & 2).

In pure methanol, **L_1** displayed a very weak emission band with an obscure maximum at around 485 nm when excited at 380 nm (Figure 1A). Emission spectra of **L_1** recorded with varying

View Article Online
DOI: 10.1039/C6NJ03070J

water fraction in a methanol-water mixed solvent revealed that though increase in the water fraction up to 70% did not induce any noticeable change in the spectral signature of L_1, further increase in the water fraction (80% or above) could lead to dramatic enhancement in its emission intensity. Meanwhile this huge TURN-ON fluorescence of L_1 in the methanol-water mixture having water content more than 80% or equal also witnessed about 25 nm red shift in the emission maxima to introduce a new emission maximum at 510 nm. L_2 followed similar trends in the fluorescence spectral behavior.

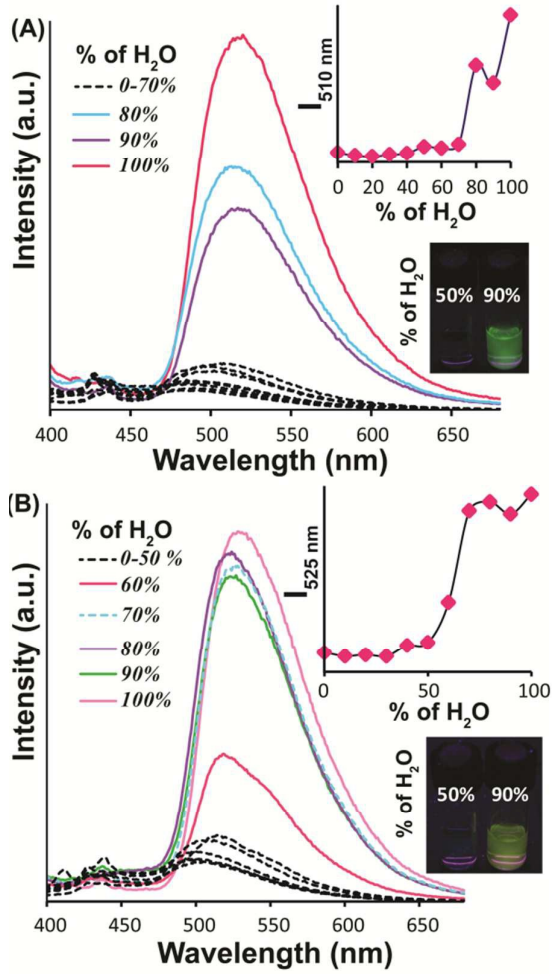

Figure 1: Fluorescence spectra of L_1 (10 μM) (A) and L_2 (10 μM) (B) upon changing the water fraction of methanol-water mixed solvent; λ_{ex} = 380 nm. INSET: change in the intensity and visual changes in fluorescence (under UV light) with different water fractions.

Upon excitation at 380 nm, L_2 also rendered a broad weak emission band at around 494 nm (Figure 1B) in methanol medium. Increase in water fraction up to 50 % in a methanol-water mixture showed very insignificant changes in the fluorescence spectra of L_2. However, further increase in the water fraction (60% or above) resulted in the unprecedented enhancement in its emission intensity accompanied by 21 nm red shift in the emission maxima and thus new emission maxima arose at 525 nm (Figure 1B). Hence, these detailed spectral studies strongly recommended that both L_1 and L_2 could demonstrate aggregation induced emission behavior. Dynamic light scattering (DLS) studies of L_1 and L_2 in a mixed aqueous medium revealed that the average particle size increased to 232 nm and 370 nm from 136 nm and 259 nm respectively (Figure S12 & S13, ESI) for L_1 and L_2 upon increasing water content of the medium from 50% to 90%. Moreover, evidence for the aggregation phenomena in methanol water mixture with higher water content (9:1 methanol-water; v/v) was strengthened by obtaining corresponding atomic force microscope images of L_1 and L_2 (Figure S14, ESI). Solid state/film state fluorescence spectra of L_1 and L_2 also authenticated the AIE active nature of these molecules by showing strong fluorescence with emission maxima at 525 nm and 548 nm respectively, when excited at 380 nm (Figure S15, ESI). Thus, beyond any doubt L_1 and L_2 are classic AIE active compounds which can display dramatic enhancement in its fluorescence as a consequence of restricted intra-molecular rotation (RIR) due to aggregation in solution or in the solid state. It also should be paid attention that due to aggregation induced emission; L_1 exhibited strong green fluorescence whereas L_2 illuminated a strong greenish-yellow fluorescence (Figure 1A & B INSET). However, as our aim was to develop a system capable of displaying white light emission, it was necessary to link AIE phenomenon with dual emission behavior (comprised of complementary emission colors). Hence we designed the molecule L_3, where we kept the bis-imine core intact with naphthol moiety which is actually responsible for the AIE behavior of these types of compounds.[23, 25] However, in place of phenyl (in L_1) or naphthyl (L_2) moiety we introduced another fluorophore (pyrene moiety) which itself can emit bluish-green fluorescence in aqueous methanol (beacause of excimer formation) to achieve effective dual emission.

Fluorescence spectroscopic studies of L_3:

In pure methanol medium, L_3 displayed two clear but very low intensity emission maxima at ~460 nm (**peak 1**) and ~516 nm (**peak 2**) upon excitation at 380 nm; which can be attributed to the presence of both pyrene and hydroxy-naphthalene moiety in the molecule (Figure 2A). It was observed that increasing water fraction of a methanol-water mixed solvent (from 0%) up to 20% led to gradual increase in the intensity of L_3, wherein the emission peak around 460 nm increased more steadily compared to the emission peak at 516 nm (Figure 2A). Interestingly, increasing water fraction from 20% to 30% not only induced certain increase in the overall emission intensity but also tempted sudden significant red shift in the emission **peak 2** from 516 nm to 556 nm whereas emission **peak 1** experienced negligible shift. Increasing the water fraction from 30% to 40% also resulted in substantial enhancement of the intensity in both of its emission peaks (**peak1** and **peak 2**) besides causing 10 nm further red shift of the emission **peak 2** from 546 nm to 556 nm. Similarly, changing the water fraction to 50% led to further red shift of its maxima (**peak 2**) from 556 nm to 570 nm along with slight growth of its intensity (**peak 2**).

View Article Online
DOI: 10.1039/C6NJ03070J

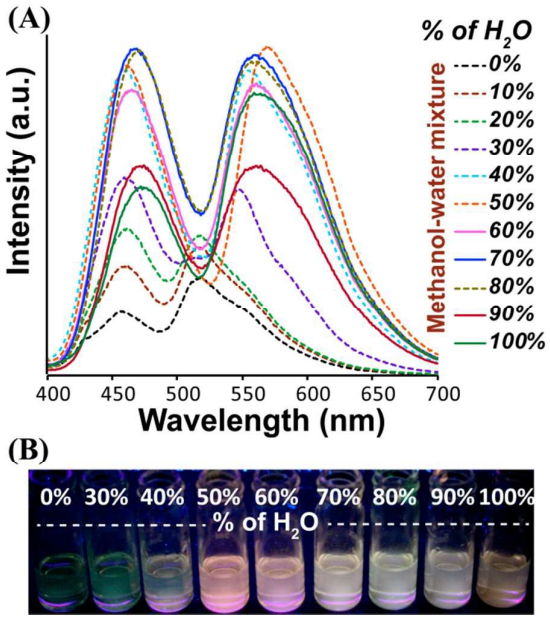

Figure 2: (A) Fluorescence spectra of L_3 (10 μM); upon changing the water fraction of methanol-water mixed solvent; λ_{ex} = 380 nm; (B) Visual changes in fluorescence (under UV light) with different water fractions.

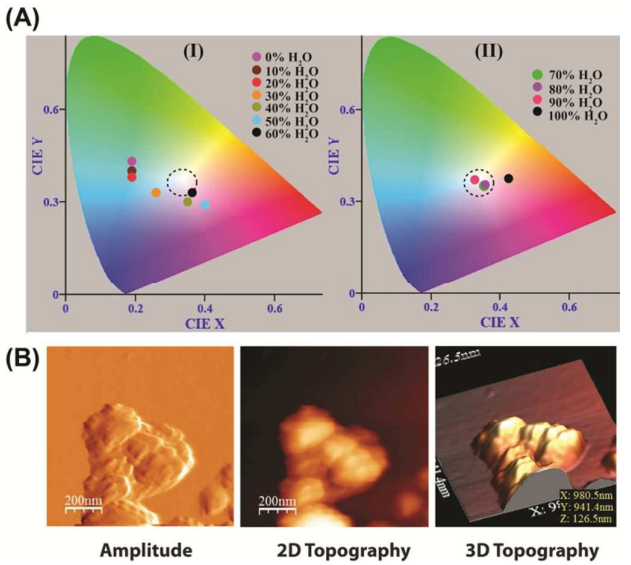

Figure 3: (A) CIE chromacity diagram of the spectra of L_3 in different water fractions [(I) 0-60% water fractions & (II) 70-100% water fractions] in methanol-water mixture; (B) AFM image of the aggregates obtained from a drop casted solution of L_3 in 9:1 methanol water solvent.

However, it was important to note that emission **peak 1**, neither showed any change in it's intensity nor experienced any shift upon changing the water fraction from 40% to 50%. Compared to 50% water fraction, in 60% water fraction L_3 witnessed slight decrease in the intensity of both of its emission maxima. Meanwhile, emission **peak 1** witnessed ~ 5 nm red shift whereas emission **peak 2** displayed ~10 nm blue shift to exhibit two emission maxima at 465 nm and 560 nm respectively upon altering the water fraction from 50% to 60%.Thereafter increasing water fraction to 70% did not show any change in the spectral nature of L_3 except causing slight enhancement in the emission intensity (Figure 2A). Increasing water fraction from 70% to 80% induced almost no change except producing very small red shift in the emission **peak 1** from 465 nm to 468 nm.

However, upon changing the water fraction to 90%, there was reasonable reduction in the overall emission intensity of L_3, accompanied by further slight (~4 nm) red shift in its emission maximum at 468 nm (**peak 1**) to facilitate emergence of a new emission maximum at 472 nm whereas the other emission peak at 560 nm (**peak 2**) remained unaltered (Figure 2A). As a result of this L_3 displayed dual emission with two distinct emission peaks at 472 nm (**peak 1**) and 560 nm (**peak 2**) with almost same intensities in methanol-water mixed solvent having 90% water content (Figure 2A). Altering water fraction from 90% to almost 100% water medium (99.99%) revealed no significant shifts in the emission maxima but the emission maximum at 472 nm reduced slightly with simultaneous substantial enhancement of the emission peak intensity at 560 nm.

White light emission and plausible mechanism:

Hence, L_3 not only can display dual emission in methanol-water mixture but also apparently could tune several emission colors due to its diverse spectral natures with varying water fractions. Photograph of the resultant experimental solution of L_3 under UV-light in methanol-water mixture with varying water content (0-100%) indeed showed that L_3 could emit various fluorescence colors with various intensities based on variation of the water percentage. As evident from the figure 2B, in 70, 80 and 90% water content L_3 emitted white fluorescence in methanol-water mixture. CIE chromacity diagram too reiterated that fluorescence spectra of L_3 with 70, 80 and 90% water content represented the white light emission (Figure 3A) with CIE-coordinates (0.35, 0.35), (0.36, 0.35) and (0.33, 0.37) respectively. However, among them, emission spectra of L_3 in 9:1 methanol-water mixture has the closest coordinates (0.33, 0.37) compared with pure white light (0.33, 0.33). Hence a white light emission was achieved from a single AIE active molecular system, developed through a step by step systematic progress in molecular design.

It is worth mentioning that when non-protic solvent acetonitrile was used instead of methanol and fluorescence spectra of L_3 were recorded in the acetonitrile-water mixture having different water fractions; it also resulted in similar spectral outcome to indicate generation of white light at 40, 50 and 60% water content (Figure 4, main manuscript and Figure S16, ESI). So, essentially white light can be obtained from the molecule L_3 in variety of solvents; which further enhances the scope of its utilization.

Interestingly, likewise the case of L_1 and L_2; DLS studies of L_3 in a mixed aqueous medium too revealed that the average particle size increased from 298 nm to 393 nm upon increasing water fraction of the medium from 50% to 90% in a methanol-

View Article Online
DOI: 10.1039/C6NJ03070J

water mixture (Figure 5). Thus undoubtedly **L_3** also formed aggregates in a methanol-water mixture with higher water contents. Alongside aggregation phenomena in methanol water mixture with higher water content (9:1 methanol-water; v/v) was further corroborated by atomic force microscope images of **L_3** (Figure 3B) aggregates. It was also noted that **L_3** can exhibit strong fluorescence in solid state/ film state (Figure S15, ESI); which further qualified the molecule as a classic AIE-gen.

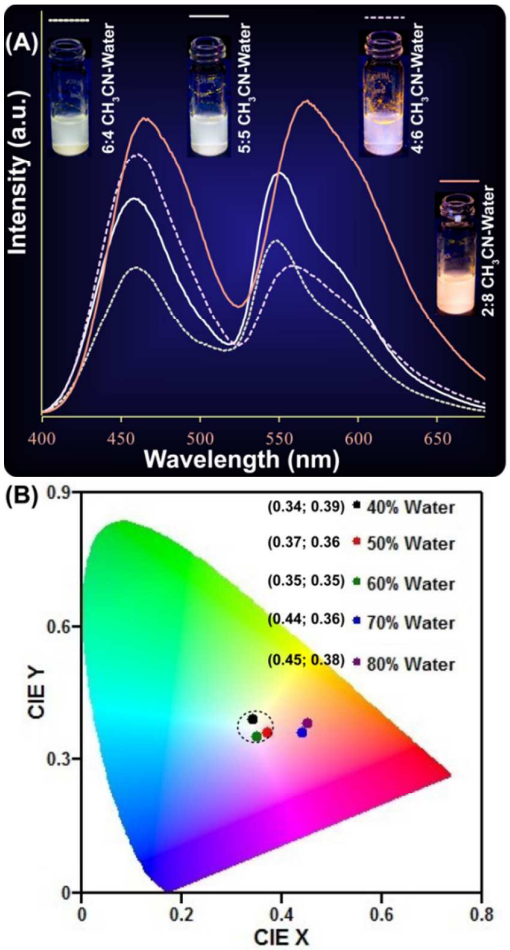

Figure 4: (A) Fluorescence spectra of **L_3** (10 μM); upon changing the water fraction of acetonitrile-water mixed solvent; λ_{ex} = 365 nm; (B) CIE chromacity diagram of the spectra of **L_3** in different water fractions in acetonitrile-water mixture.

However, even though the involvement of AIE phenomenon in the spectral outcome of **L_3** was unquestionable, the diverse spectral characters for different water fractions prompt us to suspect that some other factor(s) too might have some role in the spectral output. A close look at the structure of **L_3** suggested that it could potentially undergo ESIPT process. However it was important to understand the extent of involvement of ESIPT in influencing AIE behavior of **L_3**. The fluorescence spectra of **L_3** were recorded in solvents with varying polarity in order to verify whether proton-transfer really exists or not; and how it impacts on the excited state of **L_3**.[37-38] When the emission spectra of compound **L_3** were recorded in various solvents with different solvent polarity, there was clear red shift in the emission **peak 2** along with increase in intensity upon increasing the solvent polarity (Figure S17, ESI). This observation indicated towards the involvement of ESIPT process in the system.

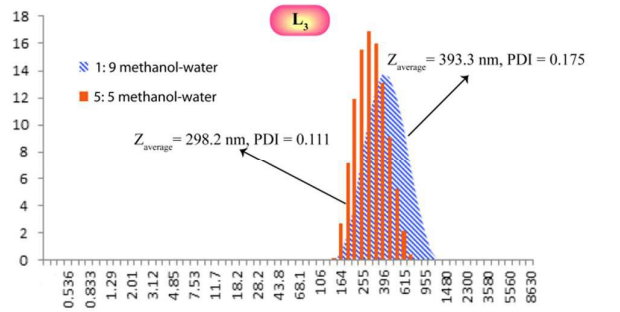

Figure 5: DLS-based particle size analysis of **L_3** (10μM) upon changing the solvent from 5:5 methanol-water to 1:9 methanol-water.

Moreover, when solvent polarity was increased by gradually increasing the water fraction (Figure 6A) of a THF-water mixed solvent (water content varied from 0% to 100%); it was interesting to note that the emission intensities of **L_3** at 510 nm increased and red shifted with the increase of the polarity of the solution (Figure 6A). This implied that a significant intramolecular electronic push–pull phenomenon exists in the bonds of N···H–O. As **L_3** is very poorly soluble in water, increasing water fraction in a methanol-water or a THF-water mixture would help aggregation (Figure 3B & 6B) of **L_3** molecules. This aggregation might restrict the intramolecular torsional motions in **L_3** to attain more planar structure which would essentially be favorable for the proton transfer from –OH to the N_{imine} atom upon photo-excitation.[37] This ESIPT process was expected to fully restrict the intramolecular rotation and help molecules of **L_3** to attain a ''lock'' structure (Scheme 3), which accounted for the gradual red shift in the band maxima (**peak 2**) from 516 to 570 nm (Figure 2A) upon increasing water fraction (up to 80%).[38]

On the other hand, it is squarely acknowledged that pyrene excimer emission λ_{em} is much less variable and generally located at 410–480 nm. Hence, **peak 1** of **L_3** (with λ_{em}~460 nm) can be attributed to the excimer formation due to the presence of pyrene moiety in it. The appearance of the excimer emission peaks in the fluorescence spectra of **L_3** may be due to close proximity of two **L_3** units at aggregated state. This assumption is also verified by taking fluorescence spectra of **L_3** at three different concentrations (1 μM, 3 μM, 5μM and 10 μM) which revealed that increase in the concentrations of **L_3** resulted in the systematic increase in the excimer peak (Figure S18, ESI). Moreover, fluorescence spectra of **L_3** taken in non-protic solvents such as hexane (poor solvent for **L_3**) and acetonitrile (moderately good solvent) revealed that even though in acetonitrile emission **peak 1** of **L_3** is absent, in hexane it can display a characteristic triple humped peak corresponding to typical pyrene moiety (Figure S19, ESI).

View Article Online
DOI: 10.1039/C6NJ03070J

Hence, emission **peak 1** can be attributed to pyrene excimer formation. Also the absence of any prominent peaks (Figure S20, ESI) in the region of 410–480 nm for L_1 and L_2 further reiterated that introducing pyrene moiety in L_3 actually embedded the extra emission peak to harvest dual emission. Hence, it would be fair to assess that introducing AIE phenomenon and excimer formation ability in the molecular system provided the scope for dual emission whereas ESIPT coupled-AIE phenomenon offered an additional handle to adjust emission wavelength of the corresponding emission peak suitably by varying solvent polarity to yield effective white light emission (Scheme 3).

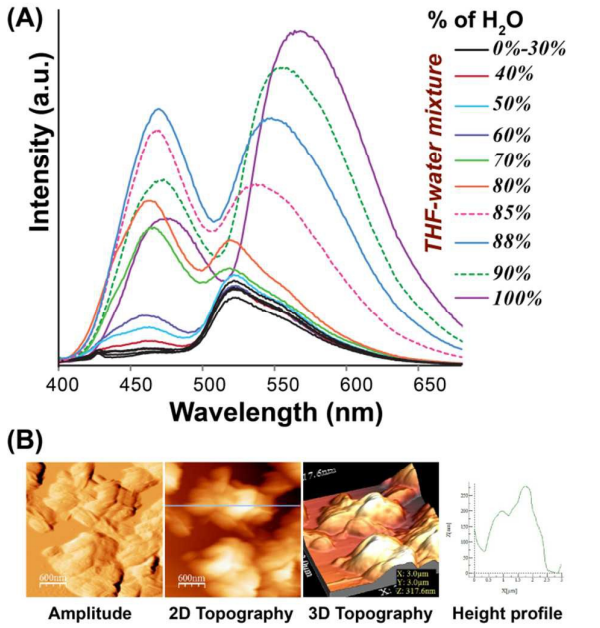

Figure 6: (A) Fluorescence spectra of L_3 (10 μM) upon changing the water fraction of THF-water mixed solvent; (B) AFM images of the aggregates obtained from the drop casted solution of L_3 (10 μM) in 1:9 THF-water mixed solvent.

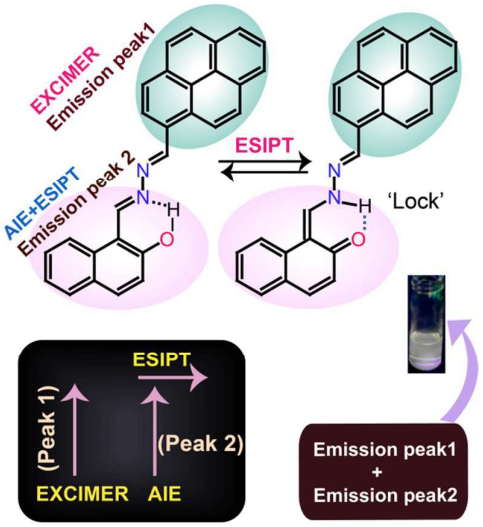

Scheme 3: Scheme for AIE-ESIPT-Excimer tripled white-light emission.

X-Ray Crystal structure of L_3:

The crystal structure of L_3 also supported the premise that AIE, ESIPT and excimer-formation are simultaneously operational in L_3 (Figure 7). We obtained the block shaped orange crystal of L_3 from DCM solvent by slow evaporation which found to be highly fluorescent in nature in the solid state itself. X-ray single crystal structure of L_3 revealed that it adopted a non-centrosymmetric molecular arrangement with a polar space group P(*2*)*1* (experimental methods). The crystal packing of L_3 suggested that two different types of orientations are present in a unit cell of L_3, which basically backed the probability of forming dimer (excimer) in solution upon aggregation (Figure 7).

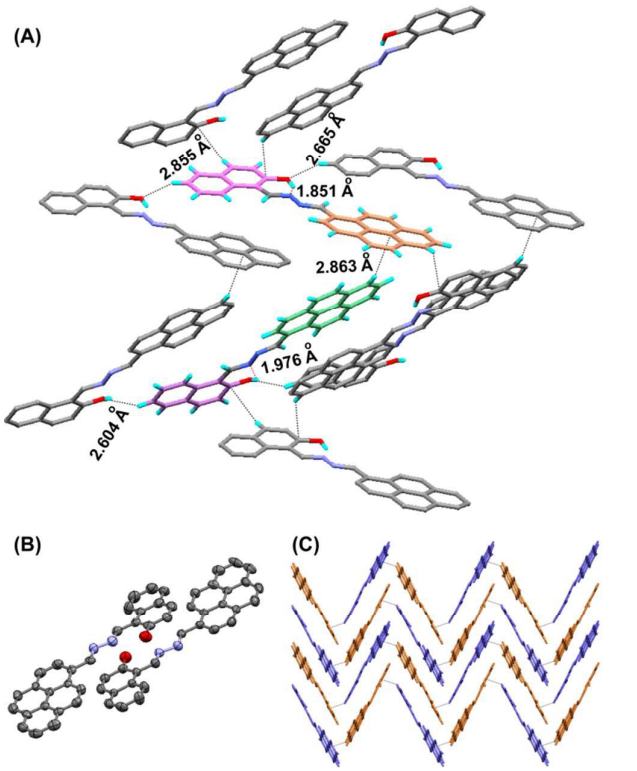

Figure 7: (A) Intra-molecular and intermolecular interactions; (B) ORTEP molecular structure and (C) molecular packing in single crystals of L_3.

One type of orientation of L_3 subjected to four intermolecular short interactions (two C–H···π & two C–H···O) whereas other type of orientation led to six intermolecular short interactions (four C–H···π & two C–H···O). It may be mentioned here that all the existed intermolecular C–H···O interactions have the distances in the range of 2.60–2.66 Å whereas intermolecular C–H···π interactions have distances in the range of 2.85–2.86 Å; which underlines the strong nature of these short interactions (Figure 7A). These types of strong interactions could be instrumental in reducing the non-radiative deactivation of excitons by locking the molecular motion in the crystal lattice.[39-40] In other words presence of the strong C–H···π & C–H···O intermolecular interactions (not π–π interactions) in L_3 helped to enhance the molecular rigidity and

View Article Online
DOI: 10.1039/C6NJ03070J

initiated its turn-on emission significantly due to the restriction of intramolecular rotation. Hence, crystal structure directly attested the AIE active nature of L_3. Besides the intermolecular interactions the single crystal of L_3 showed that there is a strong intramolecular interaction between –OH and N_{imine} which opened up the scope for a proton transfer through hexa-cyclic ring from O–H to N_{imine}. Hence more likely these interactions (both intra and intermolecular) led to the large red shift of the emission **peak 2** accompanied by gradual increase in the emission intensity upon increasing water fraction due to the formation of aggregates.

Conclusions

In summary we have systematically designed and developed of a simple organic molecule (L_3) to generate white light emission from single component. It also has the potential to tune several emission colors by varying water fractions in methanol-water mixture, due to its diverse spectral nature. Introducing aggregation-induced emission (AIE) phenomenon (**peak 2**) and excimer formation (**peak 1**) helped in securing steady enhancement in the fluorescence intensities of the respective dual emission peaks upon aggregation whereas insertion of ESIPT (excited state intramolecular proton transfer) phenomenon provided additional tool to handle the shift in emission maxima through changing solvent polarity. DLS (dynamic light scattering), AFM (atomic force microscope) Studies and crystal structure analysis directly validated the proposed lighting scheme. We hope this work would open a new window in engendering various tunable lighting applications from low cost simple single molecular devices.

Acknowledgements

G.D. acknowledges CSIR (01/2727/13/EMR-II) and Science & Engineering Research Board (SR/S1/OC-62/2011), India for financial support, CIF IITG for providing instrument facilities. SS, MB and UM acknowledge IIT Guwahati for fellowship.

References

1 C. Vijayakumar, V. K. Praveen and A. Ajayaghosh, *Adv. Mater*. 2009, **21**, 2059-2063.
2 J. Kido, M. Kimura and K. Nagai, *Science*, 1995, **267**, 1332-1334.
3 Y. Sun, N. C. Giebink, H. Kanno, B. Ma, M. E. Thompson and S. R. Forrest, *Nature*, 2006, **440**, 908-912.
4 S. Reineke, F. Lindner, G. Schwartz, N. Seidler, K. Walzer, B. Lîssem and K. Leo, *Nature*, 2009, **459**, 234-238.
5 S. Y. Lee, T. Yasuda, Y. S. Yang, Q. Zhang and C. Adachi, *Angew. Chem. Int. Ed.* 2014, **53**, 6402-6406; *Angew. Chem.* 2014, **126**, 6520-6524.
6 K. V. Rao, K. K. R. Datta, M. Eswaramoorthy and S. J. George, *Adv. Mater.*, 2013, **25**, 1713-1718.
7 Q. Chen, D. Zhang, G. Zhang, X. Yang, Y. Feng, Q. Fan and D. Zhu, *Adv. Funct. Mater.*, 2010, **20**, 3244-3251.
8 Y. Liu, M. Nishiura, Y. Wang and Z. Hou, *J. Am. Chem. Soc*., 2006, **128**, 5592-5593.
9 Q. Y. Yang and J. M. Lehn, *Angew. Chem. Int. Ed.*, 2014, **53**, 4572-4577; *Angew. Chem.* 2014, **126,** 4660-4665.
10 M. Han, Y. Tian, Z. Yuan, L. Zhu and B. Ma, *Angew. Chem. Int. Ed.*, 2014, **53**, 1090810912.
11 S. H. Kim, S. Park, J. E. Kwon and S. Y. Park, *Adv. Funct. Mater*., 2011, **21**, 644-651.
12 J. Luo, Z. Xie, J. W. Y. Lam, L. Cheng, H. Chen, C. Qiu, H. S. Kwok, X. Zhan, Y. Liu, D. Zhuc and B. Z. Tang, *Chem. Commun*., 2001, 1740-1741.
13 Y. Hong, J. W. Y. Lam and B. Z. Tang, *Chem. Soc. Rev*., 2011, **40**, 5361-5388 and references therein.
14 J. E. Kwon and S. Y. Park, *Adv. Mater*., 2011, **23**, 3615-3642.
15 J. Zhao, S. Ji, Y. Chen, H. Guo and P. Yang, *Phys. Chem. Chem. Phys*., **201**2, **14**, 8803-8817.
16 Z. Yang, W. Qin, J. W. Y. Lam, S. Chen, H. H. Y. Sung, I. D. Williams and B. Z. Tang, *Chem. Sci*., 2013,**4**, 3725-3730.
17 V. S. Padalkar, D. Sakamaki, K. Kuwada, N. Tohnai, T. Akutagawa, K. Sakai and S. Seki, *RSC Adv.*, 2016, **6**, 26941-26949.
18 J. Mei, N. L. C. Leung, R. T. K. Kwok, J. W. Y. Lam and B. Z. Tang, *Chem. Rev*., 2015, **115**, 11718-11940.
19 X. Luo, J. Li, C. Li, L. Heng, Y. Q. Dong, Z. Liu, Z. Bo and B. Z. Tang, *Adv. Mater.*, 2011, **23**, 3261-3265.
20 H. Tong, Y. Hong, Y. Dong, Y. Ren, M. Haussler, J. W. Y. Lam, K. S. Wong and B. Z. Tang, *J. Phys. Chem. B*, 2007, **111**, 2000-2007.
21 F. M. Winnick, *Chem. Rev.*, 1993, **93**, 587-614.
22 D. Sahoo, V. Narayanaswami, C. M. Kay, R. O. Ryan, *Biochemistry*, 2000, **39**, 6594-6601.
23 S. Samanta, S. Goswami, Md. N. Hoque, A. Ramesh and G. Das, *Chem. Commun.*, 2014, **50**, 11833-11836.
24 S. Samanta, C. Kar and G. Das, *Anal. Chem.*, 2015, **87**, 9002-9008
25 S. Samanta, U. Manna, T. Ray and G. Das, *Dalton Trans*., 2015, **44**, 18902-18910
26 S. Samanta, S. Goswami, A. Ramesh and G. Das, *J. Photochem. Photobiol. A*, 2015, **310**, 45-51.
27 S. Samanta, T. Ray, F. Haque and G. Das, *J. Lumin*., 2016, **171**, 13-18.
28 S. Samanta, S. Goswami, A. Ramesh and G. Das, *Sens. Actuators B.*, 2014, **194**, 120-126.
29 S. Samanta, B. K. Datta, M. Boral, A. Nandan and G. Das, *Analyst*, 2016,**141**, 4388-4393.
30 S. Samanta, P. Dey, A. Ramesh and G. Das, *Chem. Commun*, 2016, **52**, 10381-10384.
31 SAINT and XPREP, 5.1 ed.; Siemens Industrial Automation Inc.: Madison, WI, 1995. G. M.Sheldrick.
32 SADABS, empirical absorption Correction Program; University of Göttingen: Göttingen, Germany, 1997.
33 G. M. Sheldrick, SHELXTL Reference Manual: Version 5.1; Bruker AXS: Madison, WI, 1997.
34 G. M. Sheldrick, SHELXL-97: Program for Crystal Structure Refinement; University of Göttingen: Göttingen, Germany, 1997.
35 Mercury 2.3 Supplied with Cambridge Structural Database; CCDC: Cambridge, U.K., 2011 -2012.
36 S. Bhattacharya and S. K. Samanta, *Chem. – Eur. J*., 2012, **18**, 16632-16641.
37 T. He, X. T. Tao, J. X. Yang, D. Guo, H. B. Xia, J. Jia and M. H. Jiang, *Chem. Commun*., 2011, **47**, 2907-2909.
38 A. Maity, F. Ali, H. Agarwalla, B. Anothumakkool and A. Das, *Chem. Commun.,* 2015, **51**, 2130-2133.
39 A. J. Qin, J. W. Y. Lam, F. Mahtab, C. K. W. Jim, L. Tang, J. Z. Sun, H. H. Y. Sung, I. D. Williams and B. Z. Tang, *Appl. Phys. Lett*., 2009, **94**, 253308-3.
40 M. Chen, L. Li, H. Nie, J. Tong, L. Yan, B. Xu, J. Z. Sun, W. Tian, Z. Zhao, A. Qin and B. Z. Tang, *Chem. Sci.*, 2015, **6**, 1932-1937.

View Article Online
DOI: 10.1039/C6NJ03070J

Table of Contents

Rationally designed simple organic molecule exhibits white light emission in methanol/water and acetonitrile/water mixed solvents.